



## Article

# Static Hydrophobic Cuprous Oxide Surface Fabricated via One-Step Laser-Induced Oxidation of a Copper Substrate

Xi Yu <sup>1,\*</sup>, Yoshiki Tanaka <sup>2</sup>, Tomoki Kakiuchi <sup>2</sup>, Takafumi Ishida <sup>1,3</sup>, Koh Saitoh <sup>1,3</sup>, Fumihiro Itoigawa <sup>2</sup>, Makoto Kuwahara <sup>1,3</sup> and Shingo Ono <sup>2</sup>

<sup>1</sup> Institute of Materials and Systems for Sustainability, Nagoya University, Nagoya 464-8603, Japan

<sup>2</sup> Department of Engineering, Nagoya Institute of Technology, Nagoya 466-8555, Japan

<sup>3</sup> Graduate School of Engineering, Nagoya University, Nagoya 464-8603, Japan

\* Correspondence: x.yu@imass.nagoya-u.ac.jp

**Abstract:** In this study, we developed a one-step method for fabricating hydrophobic surfaces on copper (Cu) substrates. Cuprous oxide (Cu<sub>2</sub>O) with low free energy was successfully formed after low-fluence laser direct irradiation. The formation of Cu<sub>2</sub>O enhanced the hydrophobicity of the Cu substrate surface, and the contact angle linearly increased with the proportion of Cu<sub>2</sub>O. The Cu<sub>2</sub>O fabricated by low-fluence laser treatment showed the same crystal plane orientation as the pristine Cu substrate, implying an epitaxial growth of Cu<sub>2</sub>O on a Cu substrate.

**Keywords:** femtosecond laser processing; surface modification; hydrophobic surface

## 1. Introduction

Cuprous oxide (Cu<sub>2</sub>O) and copper oxide (CuO) have been investigated for photovoltaic applications [1–5] owing to their feasible bandgap (1.9–2.2 and 1.2–1.7 eV, respectively) corresponding to the visible region. Cu<sub>2</sub>O is also an emerging photocathode for water splitting [6–8]. However, there is still a need to develop low-cost methods for preparing high-quality and large-scale crystals of these promising materials [9–14]. It is more feasible to fabricate copper oxide complex thin films, which have been achieved on copper (Cu) layers via thermal oxidation for solar cells [15] and laser processing for photodetectors and glucose sensing [16,17]. Laser-treated Cu-substrate surfaces with controllable wettability have also been reported. Long et al. treated laser-fabricated microstructures with CF<sub>3</sub>(CF<sub>2</sub>)<sub>7</sub>CF<sub>2</sub>CF<sub>2</sub>–Si–(OCH<sub>3</sub>)<sub>3</sub> methanol [18], triethoxyoctylsilane [19], and fluoroalkylsilane [20] to reduce their surface free energy. Pan et al. soaked laser-textured microstructures in a stearic acid solution at ambient temperature for 60 min and dried them in an oven (60 °C) for 10 min to achieve low-adhesive features [21]. He et al. treated laser-fabricated microstructures with ethanol-assisted low-temperature annealing [22], and Ma et al. heated similar structures [23] to transform hydrophilic CuO to hydrophobic Cu<sub>2</sub>O and form hydrophobic organics. In these studies, the wettability and morphology of laser-fabricated microstructures have been extensively studied, and postprocessing was needed to add the hydrophobic base to the surface. It is also reported that a lower oxygen amount of copper-oxidation surface is associated with lower surface energy, leading to an increase in hydrophobicity [24]. Cu<sub>2</sub>O surfaces have been fabricated by chemical bath deposition [24] and electrodeposition [25,26] for achieving a hydrophobic surface. In our previous study, we developed a one-step patterning oxidation method for Cu surfaces via femtosecond laser irradiation in the atmosphere [27]. The high peak fluence due to the ultrashort pulse duration promoted the chemical reaction between Cu and oxygen. To avoid the formation of structures in the micrometer order, the samples were treated under low average fluence to suppress laser ablation. Using this one-step surface modification method, we fabricated a Cu<sub>2</sub>O layer with a thickness of less than 30 nm on the surface of a Cu substrate. Without any postprocessing, the one-step laser-treated surface showed enhanced hydrophobic features



**Citation:** Yu, X.; Tanaka, Y.; Kakiuchi, T.; Ishida, T.; Saitoh, K.; Itoigawa, F.; Kuwahara, M.; Ono, S. Static Hydrophobic Cuprous Oxide Surface Fabricated via One-Step Laser-Induced Oxidation of a Copper Substrate. *Micromachines* **2023**, *14*, 185. <https://doi.org/10.3390/mi14010185>

Academic Editor: Xin Zhao

Received: 9 December 2022

Revised: 29 December 2022

Accepted: 9 January 2023

Published: 11 January 2023



**Copyright:** © 2023 by the authors. Licensee MDPI, Basel, Switzerland. This article is an open access article distributed under the terms and conditions of the Creative Commons Attribution (CC BY) license (<https://creativecommons.org/licenses/by/4.0/>).

owing to the formation of low-free-energy  $\text{Cu}_2\text{O}$ . In addition to improving the useful time of Cu-based machine parts due to the self-cleaning feature of hydrophobic surfaces, this one-step laser-induced  $\text{Cu}_2\text{O}$  surface also showed some potential applications, such as biocides [28], photovoltaic devices [29], and photocatalysts [6].

## 2. Materials and Methods

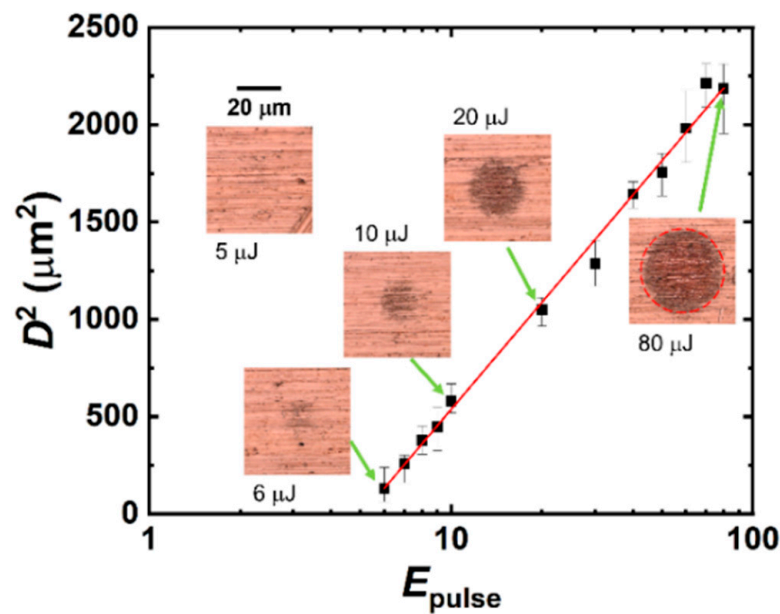
To determine the laser processing threshold of Cu substrates (113513, Nilaco, Japan), femtosecond laser pulses (wavelength: 1030 nm, pulse width: 700 fs, repetition rate: 100 kHz, PHAROS PH1–10, Light Conversion, Vilnius, Lithuania) with pulse energy of 5–60  $\mu\text{J}$  were focused and irradiated on a Cu substrate surface. The area of the single-pulse irradiated spots was measured by confocal laser scanning microscopy (CLSM, LEXT ILS4100, Olympus, Tokyo, Japan) to calculate the ablation threshold energy of Cu. Before fabricating hydrophobic samples with a large area, two 0.5 mm  $\times$  0.5 mm samples on Cu substrates were fabricated with low laser fluence. Their surface morphologies were evaluated by scanning electron microscopy (SEM, JSM-5600, JEOL, Tokyo, Japan), and their surface oxidation state was confirmed by Raman spectra (Nanofinder FLEX, TII, Tokyo, Japan). The thickness of oxidation layers was evaluated by scanning transmission electron microscopy and energy dispersive X-ray spectrometry (STEM-EDX, JEM-2100F/HK, JEOL, Tokyo, Japan). Based on the initial experimental results, samples with a size of 4 mm  $\times$  4 mm were fabricated by low-fluence laser irradiation. The surface roughness was measured by an atomic force microscope (AFM, JSPM-5200TM, JEOL, Tokyo, Japan). X-ray patterns (XRD, SmartLab, Rigaku, Tokyo, Japan), and the contact angle (CA, Smart Contact PRO 100, Excimer Inc., Yokohama, Japan) of these samples were also measured to investigate the relationship between their surface chemical composition and hydrophobicity.

## 3. Results and Discussion

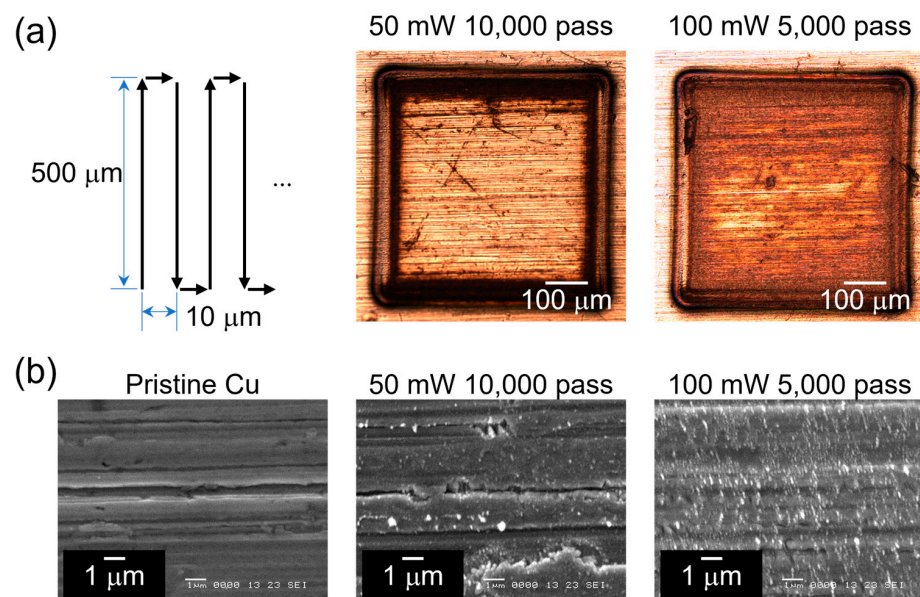
Figure 1 shows the spot diameter square ( $D^2$ ) as a function of pulse energy ( $E_{\text{pulse}}$ ). The measured  $D^2$  was fitted to  $D^2 = 2\omega_0^2 \ln \frac{E_{\text{pulse}}}{E_{\text{th}}}$ , where  $E_{\text{th}}$  is the ablation threshold energy, and the slope of the fitting is the beam radius at the surface ( $\omega_0$ ) [30]. According to the fitting result,  $E_{\text{th}}$  is 5.1  $\mu\text{J}$ , and  $\omega_0$  is 19.9  $\mu\text{m}$ . When the pulse energy is less than  $E_{\text{th}}$  (5.1  $\mu\text{J}$ ), the irradiated area shows no visible discoloration in the CLSM image. The 0.5 mm  $\times$  0.5 mm samples were irradiated by femtosecond laser pulses with an  $E_{\text{pulse}}$  of 0.5  $\mu\text{J}$  (50 mW at a 100 kHz repetition rate) and 1  $\mu\text{J}$  (100 mW at a 100 kHz repetition rate), which are much lower than  $E_{\text{th}}$ . Laser-induced plasma was not observed during the laser irradiation. The scanning patterns and their images are shown in Figure 2a. The laser beam was guided using a galvanometer scanner head, and the scan speed was 1000 mm/s with respect to the substrate surface. The scanning line space is 10  $\mu\text{m}$ . The 100 mW-irradiated area showed a more pronounced discoloration than the 50 mW-irradiated area, even though they were treated with the same total input energy. Figure 2b shows the SEM image of the pristine and laser-irradiated areas. Instead of the general microstructure fabricated by laser ablation, the low-fluence-treated surfaces showed nanoprotuberances. Mori et al. reported similar nanoprotuberances on a plasma-treated Cu surface, and they also confirmed the formation of the  $\text{Cu}^{1+}$  on the Cu surface with these nanostructures [31]. The pristine Cu showed brushing trenches on the surface, and these trenches remained after the low-fluence irradiation.

Figure 3 shows the Raman spectra of the low-fluence-treated Cu surface. The solid dots indicate the measured results. The hollow dots show the baseline-removed Raman spectrum [32], and the black line is Gaussian-fitted results from the baseline-removed Raman spectrum. Three peaks were observed for the 10,000- and 5000-pass-treated samples. Based on the fitting results, the three peaks at 216, 524, and 625  $\text{cm}^{-1}$  are attributed to  $\text{Cu}_2\text{O}$  for the second-order overtone of the silent  $\Gamma_{12}^-$  mode, the Raman-active  $\Gamma_{25}^+$  mode, and the combination mode of  $\Gamma_{12}^- + \Gamma_{25}^+$  [33–37], respectively. To confirm the crystallinity of the laser-irradiated area, we cross-sectionally picked up thin specimens from the irradiated

center of the  $500\ \mu\text{m} \times 500\ \mu\text{m}$  samples using the focused ion beam (FIB) technique (Hitachi FB2100, Japan) and evaluated them by STEM-EDX. It is difficult to identify the type of oxidation based on the measured lattice space because those of Cu,  $\text{Cu}_2\text{O}$ , and CuO are very close. EDX element mapping showed the thickness of the oxidized layer (Figure 4). Based on the mapping results, oxygen (O) layers were sandwiched between the carbon (C) and Cu layers, indicating that the oxygen was on the Cu surface before the FIB processing. A 9.7 nm-thick O layer due to natural oxidation was observed on the surface of the pristine Cu substrate. Its thickness increased by more than two times for the 50 mW-irradiated surface and three times on the surface of the 100 mW-irradiated surface. The thickness of the O layer was facilitated by laser irradiation, and higher power resulted in thicker oxidation layers owing to the longer laser penetration lengths.



**Figure 1.** Relationship between the laser pulse energy ( $E_{\text{pulse}}$ ) and the spot diameter square of the discolored area ( $D^2$ ). The discolored area is shown in the inserted CLSM images.



**Figure 2.** (a) Laser scanning pattern and images of the laser-irradiated samples. (b) SEM images of pristine, 50 mW-, and 100 mW-irradiated samples.

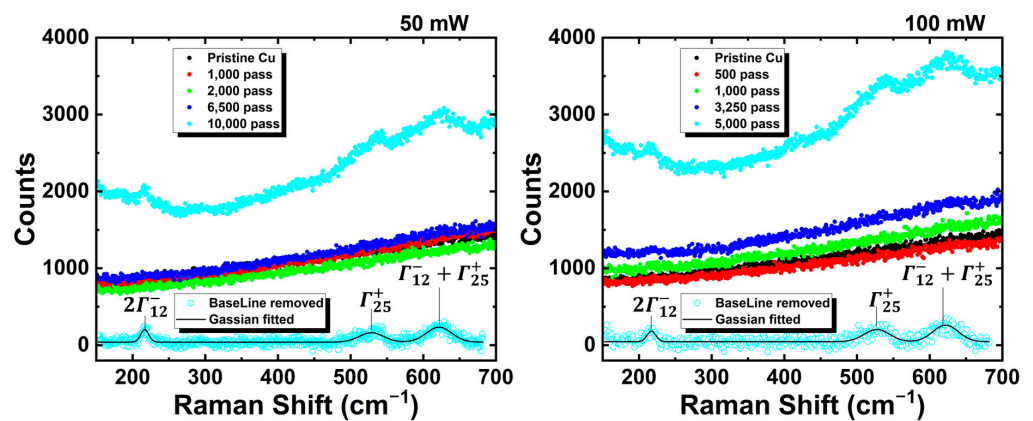


Figure 3. Raman spectra of the low-fluence laser-irradiated Cu substrate surface.

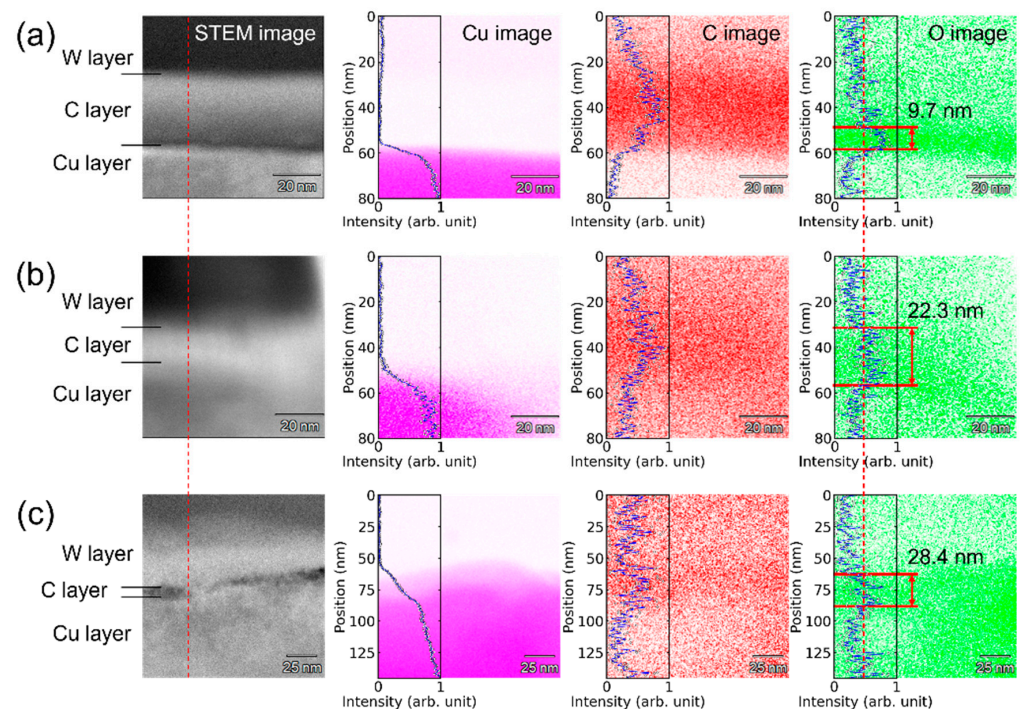


Figure 4. STEM images (cross-sectional view), Cu, C, and O mappings of (a) pristine, (b) 50 mW-irradiated, and (c) 100 mW-irradiated Cu surfaces. The red dotted line in the O image indicate the half maximum of the normalized intensity.

Table 1 shows the fabrication conditions and experiment date of laser processing, XRD, and contact angle measurement. Three samples (current samples in Table 1) with a 4 mm × 4 mm area (scanning line space: 10 μm, laser wavelength: 1030 nm, repetition rate: 100 kHz) were fabricated to evaluate the relationship between their wettability and surface oxidation conditions, and a sample from our previous study (previous sample in Table 1, fabricated using another laser with a wavelength of 1045 nm, a pulse duration of 700 fs, and a repetition rate of 100 kHz at 25 mW) [27] was also evaluated.

Figure 5a,b show the XRD pattern of the laser-irradiated Cu surfaces. The black dots indicate the measured data, and the red lines show the PseudoVoigt function fitting results [38,39]. Compared with the pristine Cu surface, a peak attributed to Cu<sub>2</sub>O (1 1 1) with a lattice spacing (*d*) of 2.09 Å was observed for all laser-irradiated samples. In Figure 5b, the Previous-1 and Previous-2 are XRD patterns with different measurement dates for the same sample from our previous work. Additionally, the Previous-1 XRD pattern shows a peak attributed to Cu<sub>2</sub>O (2 2 0) (*d*: 1.28 Å). The orientation of (2 2 0) was also observed for the pristine Cu substrate. Compared with the monoclinic structure of CuO, Cu<sub>2</sub>O has

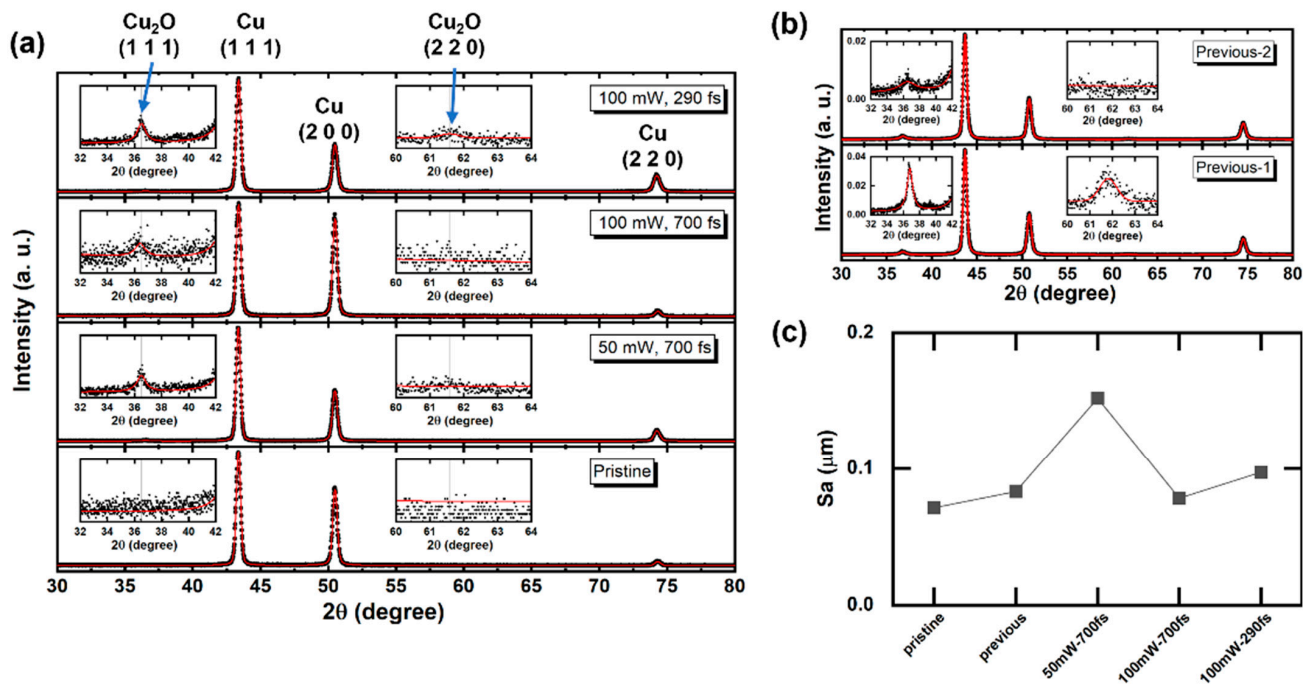
the same cubic structure as Cu, which may promote the growth of Cu<sub>2</sub>O on a Cu substrate. Barton et al. [40] reported epitaxial electrodeposition of Cu<sub>2</sub>O on single-crystal Cu owing to the similar cubic cell structures of Cu<sub>2</sub>O and Cu. They also reported that an epitaxial-grown Cu<sub>2</sub>O (2 0 0) (*d*: 1.81 Å) thin film on Cu (2 0 0) (*d*: 2.13 Å) has a thickness limitation. On a Cu (2 0 0) substrate, Cu<sub>2</sub>O (1 1 1) first grows instead of Cu<sub>2</sub>O (2 0 0), and Cu<sub>2</sub>O (2 0 0) appears when the film is thicker than 360 nm. Previous-2 showed a weaker Cu<sub>2</sub>O (1 1 1) peak than that of Previous-1 and no Cu<sub>2</sub>O (2 2 0) peak. This weakening of the Cu<sub>2</sub>O peak can be attributed to the natural oxidation of Cu<sub>2</sub>O to CuO, and the increased proportion of CuO was too low to be detected by XRD. Kwon et al. [16] reported that CuO was formed in the laser ablation center; in contrast, Cu<sub>2</sub>O was formed in the surrounding where it has lower energy density, i.e., laser fluence, than that of the center due to the Gaussian distribution of fluence. In the laser-irradiated spot, the fluence distribution determines the temperature distribution, thus determining the type of formed oxide. Lower fluence is associated with lower temperature, which facilitates the formation of Cu<sub>2</sub>O. Consequently, the low-fluence treatment in this study favored Cu<sub>2</sub>O formation. The arithmetical mean height (Sa) was used to evaluate the surface roughness as shown in Figure 5c. Sa increased less than 0.1 μm when irradiated by low laser fluence.

**Table 1.** The details of fabrication conditions and experiment date. These samples were kept in sample cases which were stored in a desiccator, and a clean tweezer was used to pick these samples when they needed to be moved.

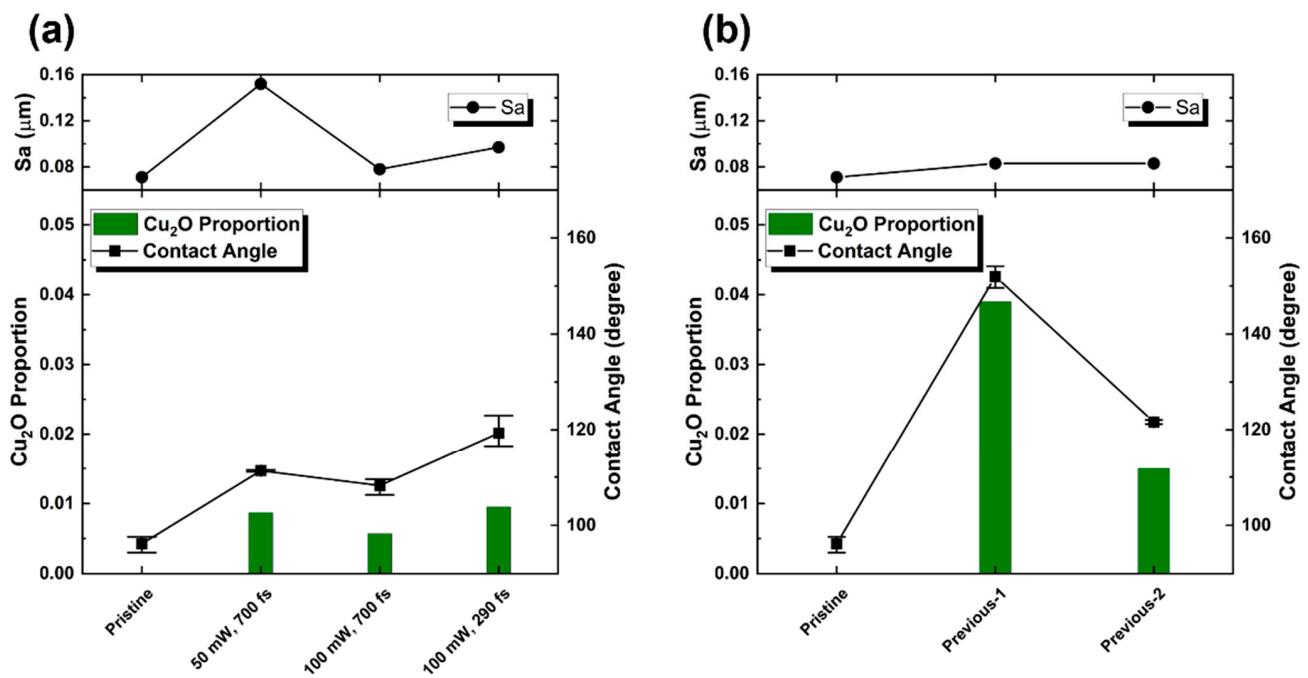
Samples	Current samples			Previous sample	
	50 mW, 700 fs	100 mW, 700 fs	100 mW, 290 fs	Previous-1	Previous-2
laser wavelength	1030 nm	1030 nm	1030 nm	1045 nm	
pulse duration	700 fs	700 fs	290 fs	700 fs	
pulse energy	0.5 μJ	1 μJ	1 μJ	0.25 μJ	
repetition rate	100 kHz	100 kHz	100 kHz	100 kHz	
scan speed	1 m/s	1 m/s	1 m/s	1.53 m/s	
scan line space	10 μm	10 μm	10 μm	22.5 μm	
fabricated date	5 April 2022	31 March 2022	18 March 2022	10 January 2018	
XRD date	12 May 2022	12 May 2022	12 May 2022	15 January 2018	12 May 2022
CA date	23–25 May 2022	23–25 May 2022	23–25 May 2022	20 July 2020	23–25 May 2022
Sa date	27 December 2022	27 December 2022	27 December 2022	27 December 2022	

Figure 6 plots the CA, Sa, and Cu<sub>2</sub>O proportion of the pristine and laser-irradiated samples. The Cu<sub>2</sub>O proportion was obtained from the ratio of the peak area (PseudoVoigt function fitting) attributed to Cu<sub>2</sub>O to that of Cu. In Figure 6a, the Sa increased by less than 0.1 μm, and in Figure 6b the Sa is almost kept the same for the pristine and the previous sample. The low-fluence laser-treated samples did not change too much in the surface roughness, which cannot significantly change the CA [25,41]. On the contrary, the proportion of Cu<sub>2</sub>O showed a positive correlation to the CAs. These results suggest that the surface free energy will be dominant to the static CA when the surface roughness insignificantly changes. Figure 7 shows the relationship between the Cu<sub>2</sub>O proportion and CA of the samples. CA increased linearly with the Cu<sub>2</sub>O proportion. The oxidation of metal copper may mitigate the surface free energy of pristine Cu, consequently enhancing the surface hydrophobicity. Meanwhile, a lower amount of oxygen results in lower surface energy [24], and Cu<sub>2</sub>O facets show different surface energies:  $E_{111} < E_{110} < E_{100}$  [42], i.e., Cu<sub>2</sub>O (1 1 1) exhibits higher hydrophobicity than other faces. In the report of Kwon et al. [43], Cu<sub>2</sub>O showed the largest CA than that of Cu and CuO due to their different interparticle bonds [44]. These results suggest that, besides the surface structure in micro-order, the chemical composition is an important factor determining the wettability

of the surface. In addition, hydrophobicity is controllable by this simple method because surface chemical compositions can be controlled by varying the laser conditions to create different reaction conditions and atmospheres.



**Figure 5.** (a) XRD patterns of current samples and a pristine Cu substrate. (b) XRD patterns of the previous sample measured on different dates with a four-year interval. (c) Surface roughness of these samples and a pristine Cu substrate.



**Figure 6.** Contact angle, Sa, and Cu<sub>2</sub>O proportion of the pristine and laser-irradiated samples. (a) 4 mm × 4 mm samples. (b) Previous sample with different experiment dates of CA and XRD. The droplets used for the CA measurement have a volume of 3  $\mu\text{L}$ . The CAs were automatically confirmed by pre-installed software which can automatically detect the edge of droplets.

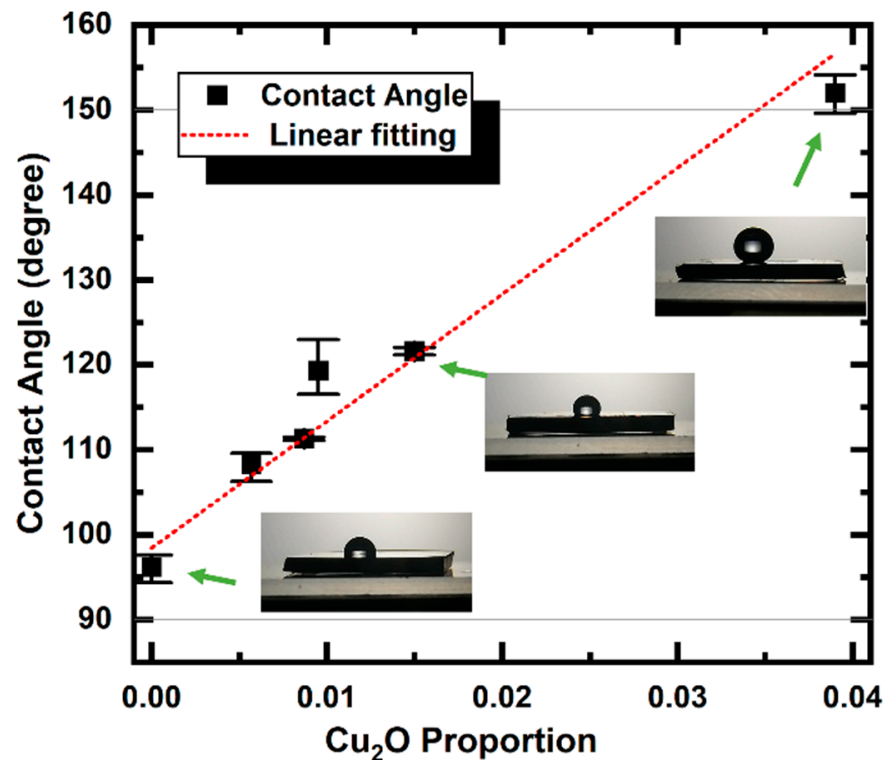


Figure 7. Relationship between Cu<sub>2</sub>O proportion and CA.

#### 4. Conclusions

In conclusion, via one-step laser irradiation, we fabricated hydrophobic surfaces on Cu substrates owing to the formation of low-free-energy Cu<sub>2</sub>O. The temperature of a laser-irradiated area could be adjusted by controlling the laser fluence, which determines the chemical composition of the copper oxides. The CA of the Cu surface exhibited enhanced hydrophobicity after the simple one-step process, showing a linear increase in the Cu<sub>2</sub>O proportion. The laser-induced Cu<sub>2</sub>O showed the same plane orientation as the Cu substrate owing to their similar cubic cell structures, implying an epitaxial growth of Cu<sub>2</sub>O on Cu. This simple one-step technique can promote the application of laser-induced functional surfaces and demonstrates the potential of laser-assisted epitaxial growth of metal oxides via direct laser irradiation in the atmosphere.

**Author Contributions:** Conceptualization, X.Y. and S.O.; methodology, X.Y., T.K., T.I., M.K.; software, X.Y.; validation, X.Y., T.K.; formal analysis, X.Y.; investigation, X.Y., Y.T., T.K., and T.I.; resources, X.Y., K.S., M.K., F.I. and S.O.; data curation, X.Y.; writing—original draft preparation, X.Y.; writing—review and editing, all the authors; visualization, X.Y.; supervision, M.K. and S.O.; project administration, M.K. and S.O.; funding acquisition, X.Y., F.I., M.K. and S.O. All authors have read and agreed to the published version of the manuscript.

**Funding:** This study was sponsored by KAKENHI (Grant No. 21H04637); Amada Foundation (Grant No. AF-2019213-B2); Iketani Science and Technology Foundation (Grant No. 0341176-A); Strategic Foundational Technology Improvement Support Operation; Grants-in-aid for the Program for Building Regional Innovation Ecosystem “Aichi Innovation Ecosystem Project for Next-Generation Automobile” from the Ministry of Education, Culture, Sports, Science and Technology of Japan; Osawa Scientific Studies Grants Foundation; Hirose Foundation.

**Data Availability Statement:** The data that support the findings of this study are available from the corresponding author upon reasonable request.

**Conflicts of Interest:** The authors declare no conflict of interest associated with this manuscript.

## References

1. Papadimitriou, L.; Economou, N.A.; Trivich, D. Heterojunction Solar Cells on Cuprous Oxide. *Sol. Cells* **1981**, *3*, 73–80. [\[CrossRef\]](#)
2. Michael, J.J.; Iniyar, S. Performance Analysis of a Copper Sheet Laminated Photovoltaic Thermal Collector Using Copper Oxide–Water Nanofluid. *Sol. Energy* **2015**, *119*, 439–451. [\[CrossRef\]](#)
3. Rakhshani, A.E. Preparation, Characteristics and Photovoltaic Properties of Cuprous Oxide—A Review. *Solid-State Electron.* **1986**, *29*, 7–17. [\[CrossRef\]](#)
4. Chandrasekaran, S. A Novel Single Step Synthesis, High Efficiency and Cost Effective Photovoltaic Applications of Oxidized Copper Nano Particles. *Sol. Energy Mater. Sol. Cells* **2013**, *109*, 220–226. [\[CrossRef\]](#)
5. Zuo, C.; Ding, L. Solution-Processed Cu<sub>2</sub>O and CuO as Hole Transport Materials for Efficient Perovskite Solar Cells. *Small* **2015**, *11*, 5528–5532. [\[CrossRef\]](#)
6. Hara, M.; Kondo, T.; Komoda, M.; Ikeda, S.; Kondo, J.N.; Domen, K.; Hara, M.; Shinohara, K.; Tanaka, A. Cu<sub>2</sub>O as a Photocatalyst for Overall Water Splitting under Visible Light Irradiation. *Chem. Commun.* **1998**, *2*, 357–358. [\[CrossRef\]](#)
7. Bagal, I.V.; Chodankar, N.R.; Hassan, M.A.; Waseem, A.; Johar, M.A.; Kim, D.-H.; Ryu, S.-W. Cu<sub>2</sub>O as an Emerging Photocathode for Solar Water Splitting—A Status Review. *Int. J. Hydrogen Energy* **2019**, *44*, 21351–21378. [\[CrossRef\]](#)
8. De Jongh, P.E.; Vanmaekelbergh, D.; Kelly, J.J. Cu<sub>2</sub>O: A Catalyst for the Photochemical Decomposition of Water? *Chem. Commun.* **1999**, 1069–1070. [\[CrossRef\]](#)
9. Mall, A.K.; Kumar, P.; Garg, A.; Gupta, R. Synthesis, Growth, and Characterizations of CuO Single Crystal. In Proceedings of the AIP Conference Proceedings, Bikaner, India, 24–25 November 2017; Volume 1953, p. 070008.
10. Bush, A.A.; Shkuratov, V.Y.; Kuz'menko, A.B.; Tishchenko, E.A. Growth and Morphological Study of Copper Oxide Single Crystals. *Crystallogr. Rep.* **2002**, *47*, 335–339. [\[CrossRef\]](#)
11. Papadimitriou, L.; Economou, N.A. Preparation of Bulk Single Crystals of Cu<sub>2</sub>O by the Plastic Flow Method and Investigation of Their Electrical Properties. *J. Cryst. Growth* **1983**, *64*, 604–608. [\[CrossRef\]](#)
12. Ebisuzaki, Y. Preparation of Monocrystalline Cuprous Oxide. *J. Appl. Phys.* **1961**, *32*, 2027–2028. [\[CrossRef\]](#)
13. Toth, R.S.; Kilkson, R.; Trivich, D. Preparation of Large Area Single-Crystal Cuprous Oxide. *J. Appl. Phys.* **1960**, *31*, 1117–1121. [\[CrossRef\]](#)
14. Su, M.; Liang, Z.; Zhao, C.; Liu, P.; Yue, S.; Xie, W. Preparation of High Quality Cu<sub>2</sub>O Crystal and Its Opto-Electronic Properties. *Mater. Lett.* **2016**, *170*, 80–84. [\[CrossRef\]](#)
15. Chen, L.-C.; Chen, C.-C.; Liang, K.-C.; Chang, S.H.; Tseng, Z.-L.; Yeh, S.-C.; Chen, C.-T.; Wu, W.-T.; Wu, C.-G. Nano-Structured CuO–Cu<sub>2</sub>O Complex Thin Film for Application in CH<sub>3</sub>NH<sub>3</sub>PbI<sub>3</sub> Perovskite Solar Cells. *Nanoscale Res. Lett.* **2016**, *11*, 402. [\[CrossRef\]](#)
16. Kwon, H.; Kim, J.; Ko, K.; Matthews, M.J.; Suh, J.; Kwon, H.J.; Yoo, J.H. Laser-Induced Digital Oxidation for Copper-Based Flexible Photodetectors. *Appl. Surf. Sci.* **2021**, *540*, 148333. [\[CrossRef\]](#)
17. Sedaghat, S.; Nejati, S.; Bermejo, L.H.; He, Z.; Alcaraz, A.M.; Roth, A.; Li, Z.; Pol, V.G.; Wang, H.; Rahimi, R. Laser-Induced Atmospheric Cu: XO Formation on Copper Surface with Enhanced Electrochemical Performance for Non-Enzymatic Glucose Sensing. *J. Mater. Chem. C* **2021**, *9*, 14997–15010. [\[CrossRef\]](#)
18. Long, J.; Fan, P.; Gong, D.; Jiang, D.; Zhang, H.; Li, L.; Zhong, M. Superhydrophobic Surfaces Fabricated by Femtosecond Laser with Tunable Water Adhesion: From Lotus Leaf to Rose Petal. *ACS Appl. Mater. Interfaces* **2015**, *7*, 9858–9865. [\[CrossRef\]](#)
19. Long, J.; Fan, P.; Zhong, M.; Zhang, H.; Xie, Y.; Lin, C. Superhydrophobic and Colorful Copper Surfaces Fabricated by Picosecond Laser Induced Periodic Nanostructures. *Appl. Surf. Sci.* **2014**, *311*, 461–467. [\[CrossRef\]](#)
20. Long, J.; Pan, L.; Fan, P.; Gong, D.; Jiang, D.; Zhang, H.; Li, L.; Zhong, M. Cassie-State Stability of Metallic Superhydrophobic Surfaces with Various Micro/Nanostructures Produced by a Femtosecond Laser. *Langmuir* **2016**, *32*, 1065–1072. [\[CrossRef\]](#)
21. Pan, Q.; Sun, B.; Liu, W.; Xue, W.; Cao, Y. Hyper Gyration Droplets Generated on a Selective Laser Textured Heterogeneous Wettability Surface. *Langmuir* **2020**, *36*, 8123–8128. [\[CrossRef\]](#)
22. He, A.; Liu, W.; Xue, W.; Yang, H.; Cao, Y. Nanosecond Laser Ablated Copper Superhydrophobic Surface with Tunable Ultrahigh Adhesion and Its Renewability with Low Temperature Annealing. *Appl. Surf. Sci.* **2018**, *434*, 120–125. [\[CrossRef\]](#)
23. Ma, L.; Wang, L.; Li, C.; Guo, J.; Shrotriya, P.; Deng, C.; Zhao, J. Hybrid Nanosecond Laser Processing and Heat Treatment for Rapid Preparation of Super-Hydrophobic Copper Surface. *Metals* **2019**, *9*, 668. [\[CrossRef\]](#)
24. Akbari, R.; Mohammadzadeh, M.R.; Khajeh Aminian, M.; Abbasnejad, M. Hydrophobic Cu<sub>2</sub>O Surfaces Prepared by Chemical Bath Deposition Method. *Appl. Phys. A* **2019**, *125*, 190. [\[CrossRef\]](#)
25. Akbari, R.; Ramos Chagas, G.; Godeau, G.; Mohammadzadeh, M.; Guittard, F.; Darmanin, T. Intrinsically Water-Repellent Copper Oxide Surfaces; An Electro-Crystallization Approach. *Appl. Surf. Sci.* **2018**, *443*, 191–197. [\[CrossRef\]](#)
26. Zhao, W.; Fu, W.; Yang, H.; Tian, C.; Li, M.; Li, Y.; Zhang, L.; Sui, Y.; Zhou, X.; Chen, H.; et al. Electrodeposition of Cu<sub>2</sub>O Films and Their Photoelectrochemical Properties. *CrystEngComm* **2011**, *13*, 2871. [\[CrossRef\]](#)
27. Yu, X.; Sudo, M.; Itoigawa, F.; Ono, S. Patterning Oxidation via Femtosecond Laser Irradiation on Copper Substrate. In Proceedings of the Conference on Lasers and Electro-Optics/Pacific Rim, Hong Kong, China, 29 July–3 August 2018; OSA: Washington, DC, USA, 2018; p. W3A.93.
28. Thomas, K.; Raymond, K.; Chadwick, J.; Waldock, M. The Effects of Short-term Changes in Environmental Parameters on the Release of Biocides from Antifouling Coatings: Cuprous Oxide and Tributyltin. *Appl. Organomet. Chem.* **1999**, *13*, 453–460. [\[CrossRef\]](#)



29. Sears, W.M.; Fortin, E. Preparation and Properties of Cu<sub>2</sub>O/Cu Photovoltaic Cells. *Sol. Energy Mater.* **1984**, *10*, 93–103. [[CrossRef](#)]
30. Yu, X.; Itoigawa, F.; Ono, S. Femtosecond Laser-Pulse-Induced Surface Cleavage of Zinc Oxide Substrate. *Micromachines* **2021**, *12*, 596. [[CrossRef](#)]
31. Mori, H.; Sakakibara, A.; Itoigawa, F. Fine Protrusion Formation on Copper Substrate Using Atmospheric-Pressure Plasma Treatment. *J. Surf. Finish. Soc. Jpn.* **2019**, *70*, 471–476. [[CrossRef](#)]
32. Zhang, Z.-M.; Chen, S.; Liang, Y.-Z. Baseline Correction Using Adaptive Iteratively Reweighted Penalized Least Squares. *Analyst* **2010**, *135*, 1138. [[CrossRef](#)]
33. Gao, H.; Zhang, J.; Li, M.; Liu, K.; Guo, D.; Zhang, Y. Evaluating the Electric Property of Different Crystal Faces and Enhancing the Raman Scattering of Cu<sub>2</sub>O Microcrystal by Depositing Ag on the Surface. *Curr. Appl. Phys.* **2013**, *13*, 935–939. [[CrossRef](#)]
34. Yu, P.Y.; Shen, Y.R. Resonance Raman Studies in Cu<sub>2</sub>O. I. The Phonon-Assisted 1s Yellow Excitonic Absorption Edge. *Phys. Rev. B* **1975**, *12*, 1377–1394. [[CrossRef](#)]
35. Yu, P.Y.; Shen, Y.R. Multiple Resonance Effects on Raman Scattering at the Yellow-Exciton Series of Cu<sub>2</sub>O. *Phys. Rev. Lett.* **1974**, *32*, 373–376. [[CrossRef](#)]
36. Compaan, A.; Cummins, H.Z. Resonant Quadrupole-Dipole Raman Scattering at the 1S Yellow Exciton in Cu<sub>2</sub>O. *Phys. Rev. Lett.* **1973**, *31*, 41–44. [[CrossRef](#)]
37. Yu, P.Y.; Shen, Y.R.; Petroff, Y.; Falicov, L.M. Resonance Raman Scattering at the Forbidden Yellow Exciton in Cu<sub>2</sub>O. *Phys. Rev. Lett.* **1973**, *30*, 283–286. [[CrossRef](#)]
38. Sánchez-Bajo, F.; Cumbera, F.L. The Use of the Pseudo-Voigt Function in the Variance Method of X-ray Line-Broadening Analysis. *J. Appl. Crystallogr.* **1997**, *30*, 427–430. [[CrossRef](#)]
39. Enzo, S.; Fagherazzi, G.; Benedetti, A.; Polizzi, S. A Profile-Fitting Procedure for Analysis of Broadened X-ray Diffraction Peaks. I. Methodology. *J. Appl. Crystallogr.* **1988**, *21*, 536–542. [[CrossRef](#)]
40. Barton, J.K.; Vertegel, A.A.; Bohannon, E.W.; Switzer, J.A. Epitaxial Electrodeposition of Copper(I) Oxide on Single-Crystal Copper. *Chem. Mater.* **2001**, *13*, 952–959. [[CrossRef](#)]
41. Li, C.; Zhang, J.; Han, J.; Yao, B. A Numerical Solution to the Effects of Surface Roughness on Water–Coal Contact Angle. *Sci. Rep.* **2021**, *11*, 459. [[CrossRef](#)]
42. Maimaiti, Y.; Nolan, M.; Elliott, S.D. Reduction Mechanisms of the CuO(111) Surface through Surface Oxygen Vacancy Formation and Hydrogen Adsorption. *Phys. Chem. Chem. Phys.* **2014**, *16*, 3036. [[CrossRef](#)]
43. Kwon, M.H.; Jee, W.Y.; Chu, C.N. Fabrication of Hydrophobic Surfaces Using Copper Electrodeposition and Oxidation. *Int. J. Precis. Eng. Manuf.* **2015**, *16*, 877–882. [[CrossRef](#)]
44. Voinea, M.; Vladuta, C.; Bogatu, C.; Duta, A. Surface Properties of Copper Based Cermet Materials. *Mater. Sci. Eng. B* **2008**, *152*, 76–80. [[CrossRef](#)]

**Disclaimer/Publisher’s Note:** The statements, opinions and data contained in all publications are solely those of the individual author(s) and contributor(s) and not of MDPI and/or the editor(s). MDPI and/or the editor(s) disclaim responsibility for any injury to people or property resulting from any ideas, methods, instructions or products referred to in the content.